Zero-field μSR measurements in *Cu*Mn and *Au*Mn spin glasses interpreted in the frame of a fractal cluster model

H. Pinkvos,* A. Kalk, and Ch. Schwink
Institut für Metallphysik und Nukleare Festkörperphysik, TU Braunschweig, Mendelssohnstrasse 3, 3300 Braunschweig, Federal Republic of Germany
(Received 5 July 1989)

We present a detailed analysis of zero-field muon-spin-relaxation (μSR) measurements in *Cu*Mn and *Au*Mn spin glasses in the framework of a fractal cluster model. The latter is reformulated in terms of a probability distribution of spin-correlation times from which an expression for the spin autocorrelation function $S(t)$ is inferred. The fractal cluster model predicts that the upper limit τ_ξ of the correlation time spectrum diverges at the freezing temperature T_f and *decreases* below T_f. The μSR method measures the average amplitude a_s of a static part and the effective correlation time $\tau_{\rm eff}$ of a rapidly fluctuating part of the local magnetic field at the muon site. The scaled quantities a_s/a_0, where a_0 denotes the static field amplitude in the limit $T\rightarrow 0$, and $\tau_{\rm eff}T_f$ turn out to be universal functions of the reduced temperature T/T_f for all investigated spin glasses. $\tau_{\rm eff}$ *decreases* below T_f and qualitatively reflects the temperature dependence predicted by the fractal cluster model for the characteristic correlation time τ_ξ. To relate the local-field time correlations and the spin autocorrelation function $S(t)$ quantitatively, we discuss two different models for the local-field dynamics as probed by μSR. As a result the μSR data do not reflect a spatial arrangement of spin clusters reorienting with size-dependent relaxation times. Rather the local field appears to be similar at each muon site and seems to consist of many contributions from different spins fluctuating with different correlation times. We analyze neutron and ac susceptibility data for the spin autocorrelation $S(t)$ within the fractal cluster model and show that they agree well with the μSR results.

I. INTRODUCTION

The spin glasses *Cu*Mn and *Au*Mn provide typical examples for the classic group of metallic systems, which consist of dilute $3d$ transition-metal impurities randomly substituted into a noble-metal host. Although both alloy systems represent similar fcc solid solutions, they differ in characteristic properties such as their tendency to short-range ordering or the magnetic anisotropy,[1] which are much larger in *Au*Mn than in *Cu*Mn.

Among the most remarkable experimental properties[1] of these spin glasses is the unusual spin dynamics at low temperatures. Below their "freezing" or "glass" temperature T_f, which is marked by a sharp cusp in the ac susceptibility,[2] spin glasses show time (or frequency)-dependent effects, whatever the time (or frequency) scale probed by the experiment. An extremely wide range of spin-correlation times between 10^{-13} and roughly 10^5 s has been investigated by a variety of dynamic experiments, e.g., neutron-spin-echo (NSE),[3-5] zero-field muon-spin-relaxation (ZF-μSR),[6-8] dynamic susceptibility ($\chi_{\rm ac}$),[9-11] relaxation of the thermoremanent magnetization,[12-14] and magnetic noise measurements.[15-18] A central quantity studied here is the time-dependent spin autocorrelation $S(t)=\langle\sigma(t)\cdot\sigma(0)\rangle$, where σ denotes the impurity spin, or the Fourier transform of $S(t)$, the magnetic noise spectrum $J(\omega)$.[19]

Since Edwards and Anderson[20] (EA) defined a new type of order parameter as the limit of the (averaged) spin autocorrelation for infinite times, dynamic methods have contributed much to the problem whether or not spin glasses undergo a genuine phase transition at T_f. Yet this question still has no definite answer. In recent years an increasing number of investigators[21-25] analyzed their results in the frame of the dynamic scaling theory of (conventional) phase transitions.[26] This concept is based on the assumption of a spin-glass correlation length ξ, which diverges at T_f as a power of the reduced temperature $\epsilon=(T-T_f)/T_f$. The experimentally observed quantities can be related to a characteristic correlation time τ_ξ, which itself is a power of the correlation length and consequently diverges at T_f.

To study the quasistatic equilibrium behavior while approaching T_f from above, it is necessary to measure dynamic properties at very long times or very low frequencies,[25] respectively. Although the scaling is generally considered to be satisfactory, the exponents found do not seem to be universal, e.g. they differ for two different metallic systems with Ruderman-Kittel-Kasuya-Yosida (RKKY) interactions.[23,25,27] In addition, it is extremely difficult to rule out other possible scaling laws, e.g., corresponding to a zero-temperature transition[28] or activated dynamic scaling.[29,30]

Things have turned out to be more complicated below T_f, where dynamic methods revealed pronounced nonequilibrium effects at long observation times (above 100 s).[31,32,14] Here the spin-glass response to a change of external field or temperature depends on the waiting time, which the system has spent in the given state before the change. Theoretical advances, which can probably

account for these effects, have been made only very recently.[33,34]

Dynamic experiments that probe short-time scales like NSE ($\approx 10^{-14}$–10^{-9} s) or ZF-μSR ($\approx 10^{-10}$–10^{-5} s) most likely cannot contribute very much to the observation of diverging spin-correlation times near T_f because of their limited time window, but for the same reason they are not hampered by nonequilibrium effects below T_f. It is therefore interesting to pursue the theoretical predictions for the low-temperature dynamical behavior and look for corresponding experimental results. Theoretical information about spin dynamics can be roughly grouped into three categories.

(1) Analytic solutions exist for the dynamic version of the EA model with infinite range interactions.[35] Unfortunately this mean field theory turned out to be inappropriate for real systems.[36,37]

(2) Knowledge about EA models with short-range interactions stems from computer simulations,[36,38,39] which mainly address problems such as the existence of a phase transition, critical dimensions, etc. Especially metallic spin-glass systems are modeled in random-site simulations of Heisenberg spins with RKKY interactions.[40,41] Although desirable, information about spin dynamics are scarce in both types of simulations with the notable exception of the $3d$ short-range Ising model,[42] where the spin autocorrelation has been characterized in detail. Here the critical exponents differ from the mean-field values, but also from those obtained experimentally for the metallic system *Ag*Mn.[25]

(3) A group of models completely different from the EA approach envisions the spin-glass transition as a percolation of spin clusters.[43–46] Some of them have been profoundly criticized.[36] An interesting and promising concept, however, is the critical fractal cluster model, which has been developed by Malozemoff together with Barbara and Continentino (MBC).[46,47] Here the adaptation of the percolation theory of phase transitions[48] to the spin-glass problem yields a variety of unusually detailed predictions for experimentally accessible quantities. The model has already been used to interpret the observed relaxation behavior of the remanent magnetization in a metallic spin-glass system.[49]

In this paper we present a detailed analysis of neutron, ac susceptibility, and zero-field μSR results of the metallic spin-glass systems *Cu*Mn and *Au*Mn in the frame of the fractal cluster model. The paper is organized as follows. In Sec. II we briefly introduce the MBC model and derive a probability distribution of spin-correlation times, from which all further quantities can be inferred. In Sec. III we use an expression for the spin autocorrelation $S(t)$ to analyze neutron and ac susceptibility data for the system *Cu*Mn and determine the model parameters for a few temperatures T/T_f. Section IV gives an introduction to ZF-μSR in spin glasses. Since μSR probes the dynamics of local magnetic fields rather than spin dynamics directly, additional assumptions are necessary to relate both. We consider two extreme cases here. In Sec. V the assumption of a spatially inhomogeneous distribution of correlation times is shown to contradict the analysis of Sec. III. In Sec. VI we turn to the opposite case that the spin autocorrelation of the MBC model describes the local-field dynamics independent of the muon site, which turns out to be in reasonable agreement with Sec. III. Section VII comments on limits of the latter interpretation in connection to the sample preparation and Sec. VIII summarizes the results.

II. THE FRACTAL CLUSTER MODEL OF MALOZEMOFF, BARBARA, AND CONTINENTINO (REFS. 46 AND 47)

The underlying physical picture in the fractal cluster model of MBC consists of rigid, noninteracting clusters, which grow in size when the temperature is lowered towards T_f. At T_f an infinite percolating network is formed and the participating spins appear to be frozen on most experimental time scales.

At a given reduced temperature $\epsilon=(T-T_f)/T_f$ (ϵ small) all relevant physical quantities are controlled by a characteristic cluster size s_ξ which relates to the correlation length ξ through $s_\xi \propto \xi^D$. Here D denotes the fractal dimension of the clusters and the correlation length is assumed to diverge, as $\xi \propto \epsilon^{-\nu}$ as usual.

The quantity of interest is the distribution of cluster sizes: the number n_s of clusters containing s spins is given by

$$n_s \propto s^{-2-1/\delta} f(s/s_\xi) \; . \tag{1}$$

The scaling function $f(y)$ approaches a constant at low values of y and falls off rapidly for $y>1$, thus expressing the fact that it is very unlikely to find a cluster with more than s_ξ spins for a given $\xi(\epsilon)$, and δ is a standard critical exponent.

Since the correlation time τ_s of a cluster is related to its size s by $\tau_s=\tau_0 s^x$, where τ_0 is a microscopic time (of the order 10^{-13} s) and x is another critical exponent, the cluster-size distribution can be converted into a distribution of correlation times $p(\tau)$. Such distributions have been assumed in general form earlier for the interpretation of ac susceptibility measurements,[11,50] but the MBC model now gives an explicit functional form. The calculation below follows approximately the treatment of Lundgren *et al.*[49]

The probability to find a spin with correlation time τ_s is given by sn_s/N, where N denotes the total number of spins. With the approximation

$$f(s/s_\xi)=\begin{cases} 1 & \text{for } s \le s_\xi \\ 0 & \text{for } s > s_\xi \end{cases} ,$$

$p(\tau)$ is given by

$$p(\tau)d\ln\tau=\begin{cases} \dfrac{1}{C}\dfrac{1}{\delta x}\left[\dfrac{\tau}{\tau_0}\right]^{1/(\delta x)} d\ln\tau & \text{for } \tau_0 \le \tau \le \tau_\xi \\ 0 \quad \text{elsewhere} \; . \end{cases} \tag{2}$$

Here and henceforth δx denotes the product δx. From the normalization conditions[46]

$$\int_{\tau_0}^{\tau_\xi} p(\tau)d\ln\tau = 1 \quad \text{for } T > T_f \ ,$$

$$\int_{\tau_0}^{\infty} p(\tau)d\ln\tau = 1 \quad \text{for } T < T_f \ ,$$

the constant C follows as

$$C = \begin{cases} 1-(\tau_0/\tau_\xi)^{1/(\delta x)} & \text{for } T > T_f \ , \\ 1 \quad \text{for } T < T_f \ . \end{cases} \tag{3}$$

To illustrate the model, the distribution $p(\tau)$ is shown in Fig. 1. The characteristic cluster size s_ξ is now replaced by the characteristic correlation time τ_ξ. Both are connected to the correlation length ξ via $\tau_\xi = \tau_0 s_\xi^x \propto \tau_0 \xi^{Dx}$. Above T_f [Fig. 1(a)] the distribution is cut off at τ_ξ. With decreasing temperature ($\epsilon \to 0$), τ_ξ diverges because the correlation length diverges and the distribution $p(\tau)$ covers all correlation times between τ_0 and infinity. The lower limit τ_0 corresponds to the single-spin-correlation time ($s=1$). At T_f the clusters percolate, forming an infinite network (the infinite cluster), which we associate with an infinite correlation time at least with respect to the time scale of the μSR method.

When the temperature is lowered below T_f, the infinite cluster incorporates the largest remaining clusters as it grows. τ_ξ now represents the correlation time of the largest cluster left "free" to rotate and decreases towards shorter times [Fig. 1(b)]. The fraction of spins bound to the infinite cluster is represented by the shaded area in Fig. 1(b) and gives the order parameter q of this model:

$$q = (\tau_0/\tau_\xi)^{1/(\delta x)} \quad \text{for } \epsilon < 0 \ . \tag{4}$$

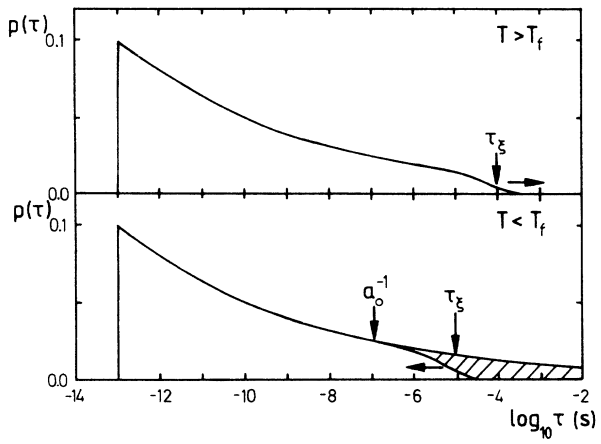

FIG. 1. Probability distribution of spin-correlation times $p(\tau)$ [Eq. (2)] inferred from the critical fractal cluster model of MBC (Refs. 46 and 47). Above T_f the distribution is cut off at the characteristic correlation time τ_ξ, which diverges as T approaches T_f. Below the freezing temperature τ_ξ *decreases* because the infinite cluster formed at T_f incorporates the largest remaining clusters as the temperature decreases. The shaded area represents the order parameter q of the fractal cluster model. The quantity a_0^{-1} sets a time scale for the muon by dividing the correlation time spectrum into a static part ($\tau > 1/a_0$) and a dynamic part ($\tau < 1/a_0$).

The quantity a_0^{-1} denotes the so-called reciprocal static linewidth and sets an important time scale for the muon, because it separates the "dynamic" part of the correlation time spectrum ($\tau < a_0^{-1}$) from the "static" part ($\tau > a_0^{-1}$). These notions are more precisely discussed in Sec. V.

III. ANALYSIS OF NEUTRON AND χ_{ac} DATA

In a first step we applied the fractal cluster model to the neutron-spin-echo (NSE) measurements of Mezei and Murani.[3-5] The NSE method directly measures the spin autocorrelation function $S(\mathbf{q},t)$ for discrete times in the range 5×10^{-12}–5×10^{-9} s. Generally it depends on the momentum transfer $\mathbf{q}$ of the neutron, but it has been argued,[4,51] that the weak q dependence found for the *Cu*Mn system permits comparison to both susceptibility measurements (χ_{ac}), i.e., the $\mathbf{q}\to0$ limit, and μSR data which correspond to a broad average over all $\mathbf{q}$.

Within the fractal cluster model the spin autocorrelation function $S(t)$ for the impurity moments is given by the integral

$$S(t) = \int_0^\infty p(\tau)e^{-t/\tau}d\ln\tau \ . \tag{5}$$

Inserting $p(\tau)$ from Eq. (2) we can approximately integrate Eq. (5) to yield for $T > T_f$

$$S_d(t) = \frac{1}{C}\{[1-(\tau_0/t)^{1/(\delta x)}]\exp(-t/\tau_0) + [(\tau_0/t)^{1/(\delta x)} - (\tau_0/\tau_\xi)^{1/(\delta x)}]\exp(-t/\tau_\xi)\} \ . \tag{6}$$

The constant C is again given by Eq. (3) and the subscript d (dynamical) indicates that there are no time-independent parts of $S(t)$, since τ_ξ has not diverged and

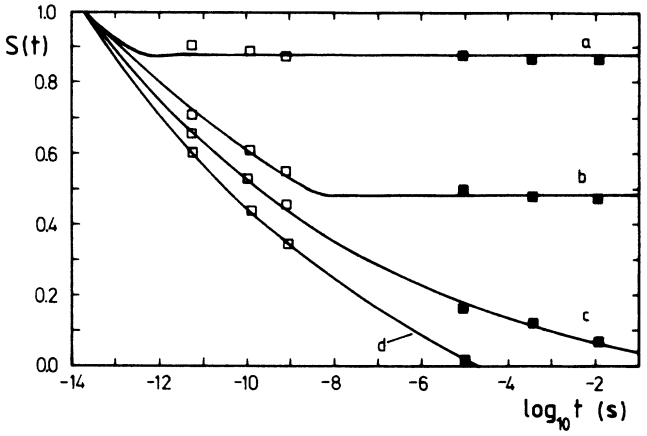

FIG. 2. Spin-autocorrelation function $S(t)$ measured by neutron scattering (open squares) and ac susceptibility (solid squares) for a *Cu*Mn(3 at. %) spin glass at temperatures $T/T_f =$ (a) 0.25, (b) 0.75, (c) 0.9, and (d) 1.0 (data taken from Ref. 5). The solid lines correspond to least-squares fits of the model functions Eqs. (6) and (7), which are derived from the fractal cluster model (see text).

TABLE I. Model parameters of the spin autocorrelation $S(t)$ of the fractal cluster model obtained from least-squares fits of Eqs. (6) and (7) to the neutron and χ_{ac} data shown in Figs. 2 and 3.

Symbol	T/T_f	τ_0 (s)	τ_ξ (s)	δx	Equation
*Cu*Mn(1 at. %)		$T_f=9.9$ K	Fig. 3		
a	0.8	1×10^{-13}	$(2.7\pm0.1)\times10^{-8}$	11±0.4	(7)
b	1.23	$(1.5\pm0.5)\times10^{-13}$	$(6\pm3)\times10^{-9}$	7±3	(6)
*Cu*Mn(3 at. %)		$T_f=20$ K	Fig. 2		
a	0.25	2×10^{-14}	$(3\pm1)\times10^{-10}$	70±20	(7)
b	0.75	2×10^{-14}	$(7\pm2)\times10^{-9}$	18±0.6	(7)
c	0.9	$(2\pm1)\times10^{-14}$	$(7\pm3)\times10^{0}$	16±2	(6)
d	1.0	$(2\pm1)\times10^{-14}$	$(3\pm1)\times10^{-4}$	18±4	(6)

consequently no contribution from the infinite cluster exists.

For $T<T_f$ the calculation gives

$$S(t)=q+(1-q)S_d(t)\ , \tag{7}$$

with q given by Eq. (4) and $S_d(t)$ by Eq. (6).[52] The above formulas require τ_ξ to be at least 3–4 orders of magnitude larger than τ_0 because expressions such as $(t/\tau)\exp(-t/\tau)$ have been treated similar to a δ function, $\delta(\tau-t)$, under the integral in Eq. (5).[49,53] For a very broad distribution the function $S_d(t)$ practically follows a power law

$$S_d(t)\approx\frac{1}{C}(\tau_0/t)^{1/(\delta x)} \tag{8}$$

if $\tau_0<t<\tau_\xi$ and $\ln\tau_\xi\gg\ln\tau_0$.

Figures 2 and 3 show neutron data for $S(t)$ combined with ac susceptibility data as given by Murani[5] for a *Cu*Mn(3 at. %) sample (Fig. 2) and by Murani *et al.*[54] for a *Cu*Mn(1 at. %) sample (Fig. 3). The latter is important, since concentrations around 1 at. % are also used in the μSR measurements. The solid lines correspond to least-squares fits of Eqs. (6) and (7) to the data. The parameters are given in Table I.

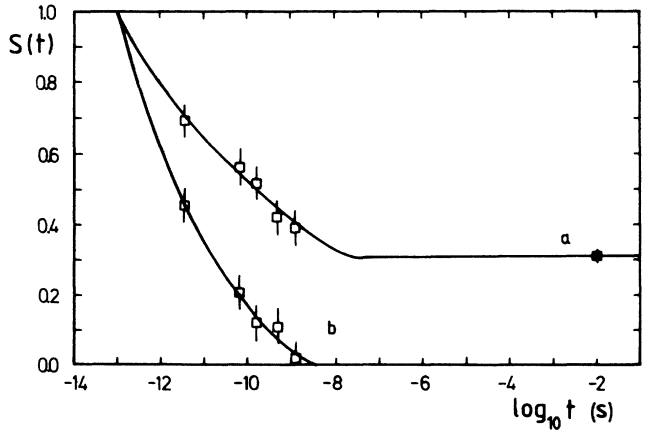

FIG. 3. Spin autocorrelation function $S(t)$ measured by neutron-spin-echo (open squares) and ac susceptibility (solid square) for *Cu*Mn(1 at. %) at temperatures $T/T_f=$ (a) 0.8 and (b) 1.23 (data taken from Ref. 54). As in Fig. 2 solid lines correspond to least-squares fits of Eqs. (6) and (7) to the data.

From the fractal cluster model we expect that data for a given concentration can be described with a common exponent δx and a common lower limit of the correlation time spectrum, τ_0, the upper limit of the spectrum τ_ξ being the only temperature dependent quantity. Table I shows that this is indeed possible within some limitations. The errors given in Table I have to be taken with care, because Figs. 2 and 3 do not contain enough data points to permit a correct χ^2 analysis. The fit favors large values for the exponent $\delta x\approx10$ for *Cu*Mn(1 at. %), which are in reasonable agreement with $\delta x=7.8\pm2$ found for the system *Ag*Mn.[24,25] Neutron and χ_{ac} data for a *Cu*Mn(5 at. %) sample[3] could not be fitted with a common τ_0, but also gave values around 10 for the exponent δx. This is in contrast with the results of Heffner and MacLaughlin,[51] who analyzed the data set restricted to the NSE part and obtained the mean-field value $\delta x=2$ below T_f and $\delta x=4$ at T_f.[55] Clearly more data with improved precision are required to draw further conclusions.

For the moment we will use Table I as a suitable parametrization of the measured spin autocorrelation, which will enable a quantitative comparison to the μSR results in the following sections.

IV. ZERO-FIELD μSR IN SPIN GLASSES

Contrary to the NSE method, the muon-spin-relaxation technique does not give direct access to the impurity spin autocorrelation in spin glasses. Rather the positive muon provides an excellent probe for the local magnetic field at interstitial sites, whose observed dynamic properties can then be related to the impurity spin dynamics.

The details of the μSR method including spin glass and many non-spin-glass applications have been described in a number of reviews[56–61] and a recent book.[62] Usually time differential histograms of positrons are recorded, which are generated in the parity violating, spatially anisotropic muon decay. From the positron spectra the muon-spin-relaxation function $G(t)$ can be deduced,

which carries the important information in the case of spin glasses. The measurements discussed below have been done at the muon channels $\mu E1$ and $\mu E4$ at the Paul Scherrer Institute [the former Swiss Institute for Nuclear Research, (SIN)] in Villigen, Switzerland with a conventional μSR spectrometer.

In the fcc lattices of the host metals Cu and Au the muon does not diffuse in the temperature range 2–70 K and samples all possible interstitial sites randomly.[62–64] The local magnetic field causes the muon spin to evolve in time and the spin-relaxation function $G(t)$ reflects in a characteristic way the distribution of the local magnetic fields and their dynamics because it is not obscured by motion of the muon.

The general appearance of $G(t)$ in the two spin-glass systems *Au*Mn and *Cu*Mn is shown in Figs. 4 and 5 for several reduced temperatures T/T_f.

In the system *Au*Mn (Fig. 4) the Mn moments provide the only source for the magnetic field. At temperatures above T_f the relaxation function follows the so-called "exponential-root" law:

$$G(t)=\exp[-(\lambda t)^{1/2}] . \tag{9}$$

This form is a direct consequence of rapidly fluctuating magnetic moments in combination with their large dilution. Owing to the random occupation of lattice sites by the Mn moments, their many possible orientations and their low concentration, the muons experience a large number of different environments, which have to be taken into account in a proper average. Such a configuration average has been explicitly treated by McHenry, Wernick, and Silbernagel[65] in the case of rapidly fluctuating moments, where the exponential-root law follows, and by Walstedt and Walker[66] and by Mikaelyan and Smilga[67] in the case of static moments, where the resulting probability distribution of the local-field amplitudes turns out to have a Lorentzian form.

The relaxation rate λ in Eq. (9) can be expressed as[7,68]

$$\lambda=4a_0^2\tau , \tag{10}$$

where $a_0=\gamma_\mu b_0$ is given by the full width at half maximum (FWHM) b_0 of the Lorentzian field distribution times the muons gyromagnetic ratio γ_μ, and τ denotes the correlation time of the local field. Equations (9) and (10) require the "narrowing" condition $a_0\tau \ll 1$ to be fulfilled.

When the temperature is lowered towards T_f the correlation time increases and consequently the relaxation rate λ increases too. A qualitative change in the appearance of $G(t)$ occurs below T_f: The relaxation function no longer decreases monotonically, but shows a minimum at short times (around 0.2 μs). This minimum unambiguously signals the presence of quasi-static local fields,[69] i.e., now $a_0\tau \gg 1$. For completely static Lorentzian distributed fields the relaxation would follow the function:[67,70]

$$G(t)=\tfrac{1}{3}+\tfrac{2}{3}(1-a_0t)\exp(-a_0t) , \tag{11}$$

which is indicated in Fig. 4 for $T=0.5T_f$.

The decay of the "$\frac{1}{3}$ tail" at long times ($t>0.3$ μs) shows, that even at $T=0.5T_f$ fluctuations of the local field are present. Without further assumptions different interpretations of this decay are possible, e.g., complete but slow reorientation of the local field,[6,7] rapid fluctuations in a small-angle interval,[7,68,71] and even a superposition of both.[72]

The relaxation function in *Cu*Mn spin glasses (Fig. 5) appears to be very similar to that in *Au*Mn at low temperatures, but different above T_f. This difference simply originates from the presence of the Cu nuclear moments. Their high concentration in combination with random

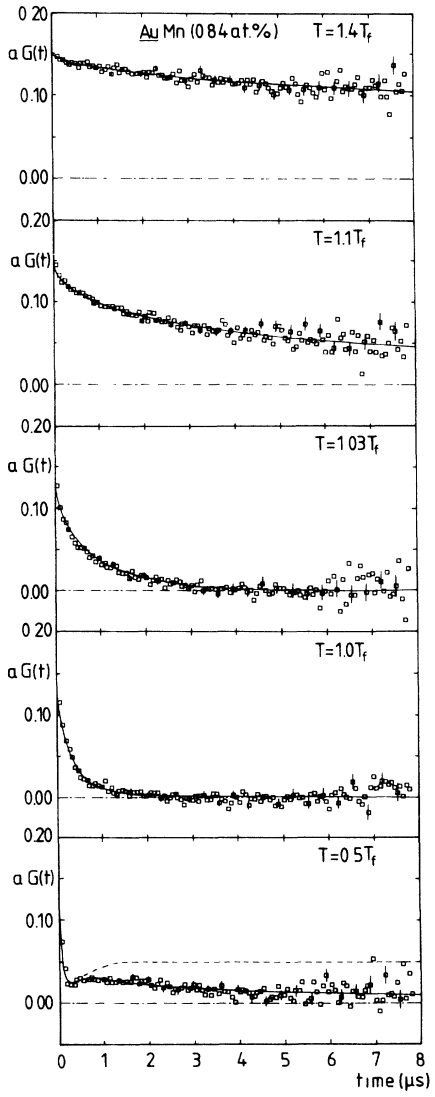

FIG. 4. Muon-spin-relaxation function $G(t)$ measured in a *Au*Mn(0.84 at. %) spin glass at several reduced temperatures T/T_f (the ordinate is scaled by the observed muon decay asymmetry a). Solid lines correspond to least-squares fits of a model function which is discussed in Sec. VI. At $T=0.5T_f$ the dashed line indicates the theoretical form of $G(t)$ for completely frozen local fields [Eq. (11)].

orientations leads to a Gaussian shape for the field distribution,[73] which contrasts to the Lorentzian form characterizing the fields of the electronic Mn moments. At $T \gg T_f$ the relaxation almost completely follows the well-known "Kubo-Toyabe" (KT) formula:[74]

$$G^{KT}(t)=\tfrac{1}{3}+\tfrac{2}{3}(1-\sigma^2t^2)\exp(-\sigma^2t^2/2)\ , \qquad (12)$$

where in our case $\sigma=\sigma_{Cu}=0.36-0.38\ \mu s^{-1}$.[62,75]

As long as the impurity moments fluctuate rapidly, they can be regarded as an independent relaxation source for the muon spin[68] and the total relaxation function is given by the product of Eq. (9) with Eq. (12). At temperatures well below T_f the quasistatic fields from the Mn moments dominate the Cu nuclear dipole fields completely and therefore the latter no longer have to be taken into account.

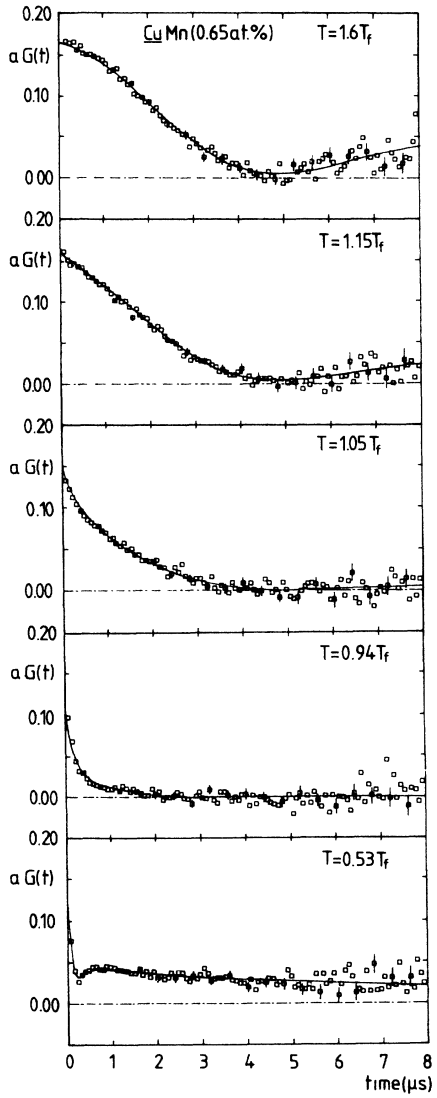

FIG. 5. Relaxation function $G(t)$ measured in a *Cu*Mn(0.65 at. %) spin glass at temperatures comparable to those of Fig. 4. The different form of the curves above T_f displays the characteristic signature of the Cu nuclear dipoles.

References 65–67 provide examples, where it has been possible to calculate the muon-spin-relaxation function directly from the dynamic properties of the impurity spins and their coupling to the muon in limiting cases. Unfortunately, no generalization to the complicated spin dynamics in the vicinity of T_f is known. Usually one calculates the relaxation function in an intermediate step using stochastic models for the local magnetic field such as the strong collision model[76,77,60] or the assumption of a Gaussian process.[74] These involve properties such as the local-field autocorrelation $S_H(t)=\langle H(t)H(0)\rangle/\langle H^2(0)\rangle$ and the static field distribution $p(H)$. The connection to the neutron results and the fractal cluster model then requires a relation between the local-field dynamics and the impurity spin dynamics, which is not straightforward.

The coupling between muon and impurity spins is mediated through two essential mechanisms: dipolar coupling and spin-density oscillations of conduction-band electrons, i.e., the RKKY interaction. For *Cu*Mn the dipole fields have been shown to dominate the RKKY fields by far.[78] Although this is not necessarily the case for other hosts such as Ag or Au, the assumption of pure dipolar fields accounts satisfactorily for the observed static Lorentzian linewidths a_0 in zero-field μSR measurements (c.f. Refs. 7 and 79, see also below). Since the dipolar coupling is anisotropic and long ranged (see, e.g., Refs. 73 and 77), the local-field autocorrelation and the impurity spin autocorrelation cannot be directly inferred from each other. Therefore we will explicitly assume here, that the local-field autocorrelation, averaged over the entire system, and the impurity spin autocorrelation measured by NSE can be directly compared, which has been discussed by Heffner and MacLaughlin[51] and implicitly assumed by Uemura *et al.*[80]

Since the muon is a localized probe, we have to specify the fluctuations of the magnetic field at a given site, calculate a local relaxation function, and perform the average over all interstitial sites. We will consider here two extreme cases.

(a) Spatially inhomogeneous local-field dynamics. Remembering that the fractal cluster model assumes rigidly coupled clusters, we may visualize the local field as fluctuating predominantly with the particular correlation time of a given cluster within its volume. The local-field autocorrelation will then be exponential, but the correlation time differs for sites belonging to different clusters.

(b) Spatially homogeneous local-field dynamics. Alternatively we can argue that the local field at a given site is a superposition of many contributions from spins belonging to different clusters because of the long-ranged coupling. This could lead to very similar fluctuations of the local field at different sites. The local-field autocorrelation will clearly be nonexponential and we may try to use the impurity spin autocorrelation discussed in Sec. III.

V. SPATIALLY INHOMOGENEOUS LOCAL-FIELD DYNAMICS

The situation requires the calculation of a local relaxation function for an arbitrary correlation time τ and a

subsequent average over the distribution $p(\tau)$ given by Eq. (2). Apart from the local-field *dynamics* we have to take into account the random variation of the local-field *amplitudes* due to the varying configuration of Mn moments around the muon sites. We will treat the problem within a scheme proposed by Uemura *et al.*:[6,68,80] The local relaxation function $G^{\rm loc}(t,\Delta,\tau)$ is calculated from the "Gaussian strong collision model"[76,77,60] for a given (local) Gaussian linewidth Δ and correlation time τ of the magnetic field and in general cannot be represented analytically. The configuration average in Refs. 65–67 is replaced by an integration over a probability distribution $\rho(\Delta)$ for the Gaussian linewidths:

$$\rho(\Delta)=(2/\pi)^{1/2}a_0/\Delta^2\exp[-a_0^2/(2\Delta^2)] \ . \tag{13}$$

The probability distribution $p(H)$ for the entire system is then Lorentzian with a FWHM $b_0=a_0/\gamma_\mu$.

The total relaxation function is given by the integral

$$G^{\rm tot}(t)=\int_0^\infty d\ln\tau\, p(\tau)\int_0^\infty d\Delta\,\rho(\Delta)G^{\rm loc}(t,\Delta,\tau) \ , \tag{14}$$

where we have assumed that the average amplitude Δ of the local field is independent of its correlation time τ. It is not clear whether this is reasonable in spin glasses, but no theoretical help exists here and we have no other argument than simplicity. If the averages are independent, the integration over Δ leads to the "Lorentzian strong collision" model.[6,68,80] The latter can be expressed analytically in two limiting cases:

$$\text{(i) } a_0\tau\ll 1\text{: } G_d^{Cl}(t)=\exp[-(4a_0^2\tau t)^{1/2}] \ , \tag{15}$$

$$\text{(ii) } a_0\tau\gg 1\text{: } G_{qs}^{Cl}(t)=[\tfrac{1}{3}+\tfrac{2}{3}(1-a_0t)\exp(-a_0t)]\times\exp(-\tfrac{2}{3}t/\tau) \ . \tag{16}$$

Equations (15) and (16) demonstrate that the reciprocal static linewidth $1/a_0$ sets a time scale for the muon by separating the region of small correlation times (fast fluctuations, "dynamic clusters") from the region of large correlation times (slow fluctuations, "quasistatic clusters") in the spectrum.[81] This is also indicated in Fig. 1.

Both approximations do not work in the vicinity of $\tau=a_0^{-1}$, but the error resulting from their use in Eq. (14) reduces with increasing width of the distribution $p(\tau)$: The spectral weight of correlation times around a_0^{-1} should play a minor role, if $\ln\tau_\xi\gg\ln\tau_0$. Inserting Eqs. (15) and (16) into Eq. (14) the remaining integration over τ can be finally performed in a way similar to the treatment of Eq. (2). The result can be expressed for $T>T_f$ as[82]

$$G^{\rm tot}(t)=G_d(t)+G_{qs}(t) \ , \tag{17}$$

where

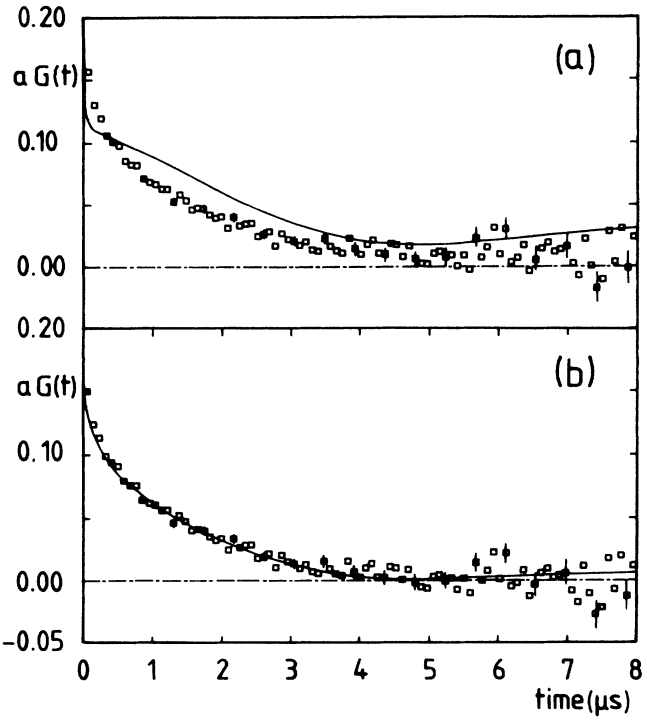

FIG. 6. Attempts to fit the relaxation function for spatially inhomogeneous local-field dynamics [Eq. (17)] to data for a *Cu*Mn(1.21 at. %) spin glass at $T=1.04T_f$. (a) τ_0 fixed at 10^{-13} s: the fit favors extremely large values for $\delta x\approx 168$ and $\tau_\xi=5\times10^{-3}$ s. (b) δx fixed at $\delta x=10$, both limits τ_0 and τ_ξ of the correlation time spectrum left as free parameters: the fit improves considerably.

$$G_d(t)=\frac{1}{C}\{\exp[-(\lambda_0 t)^{1/2}] -(\lambda_0/\lambda_\xi)^{1/(\delta x)}\exp[-(\lambda_\xi t)^{1/2}] -(\lambda_0 t)^{1/(\delta x)}\{\exp[-(\lambda_0 t)^{1/2}] -\exp[-(\lambda_\xi t)^{1/2}]\}\}$$

and

$$\lambda_0=4a_0^2\tau_0, \quad \lambda_\xi=\begin{cases}4a_0^2\tau_\xi & \text{if } \tau_\xi\le a_0^{-1} \ ,\\ 4a_0 & \text{if } \tau_\xi>a_0^{-1} \ .\end{cases}$$

The contribution from the quasistatic clusters $G_{qs}(t)$ is only finite if $\tau_\xi>a_0^{-1}$. Then

$$G_{qs}(t)=\frac{1}{C}\left\{\left[(a_0\tau_0)^{1/(\delta x)}-\left[\frac{3}{2}\frac{\tau_0}{t}\right]^{1/(\delta x)}\right]\exp(-\tfrac{2}{3}a_0t)-\left[\left[\frac{\tau_0}{\tau_\xi}\right]^{1/(\delta x)}-\left[\frac{3}{2}\frac{\tau_0}{t}\right]^{1/(\delta x)}\right]\exp\left[-\frac{2}{3}\frac{t}{\tau_\xi}\right]\right\}g_L(t,a_0) \ ,$$

where C denotes the normalization constant from Eq. (3) and $g_L(t,a_0)$ is the static "Lorentzian Kubo-Toyabe" function[67,70] given in Eq. (11). In both cases C is again given by Eq. (3).

Equation (17) gives the final formula for the muon-spin-relaxation function corresponding to the fractal cluster model with the assumption of spatially inhomogeneous local-field dynamics above T_f. Even the first trials showed that it is impossible to fit the measured relaxation functions above T_f with the strategy pursued in the analysis of the neutron data, i.e., with a common value for τ_0 and δx. Figure 6 gives an example for a *Cu*Mn(1.21 at. %) spin glass. The fits considerably improve if the exponent δx is fixed and both limits of the correlation time spectrum τ_0 and τ_ξ are left as free parameters [Fig. 6(b)]. Both limits increase by several orders of magnitude when T_f is approached (Fig. 7). This corresponds to a shift of the entire correlation time spectrum in Fig. 1 to larger times which can also be described by a single average correlation time (c.f. Sec. VI).

It is interesting to note that the data in Fig. 7 contradict the analysis of the neutron data in Sec. III. This can be seen by calculating the *averaged* local-field autocorrelation $S_H(t)$ using Eq. (6) with the parameters from Fig. 8. The comparison to the impurity spin autocorrelation $S(t)$ is shown in Fig. 8. The neutron measurements clearly suggest that for temperatures in the range 1.3–0.8 T_f a part of $S(t)$ always decays below 10^{-11} s, whereas the μSR results in Fig. 7 show *no* decay of $S_H(t)$ within this time range for $T<1.1T_f$.

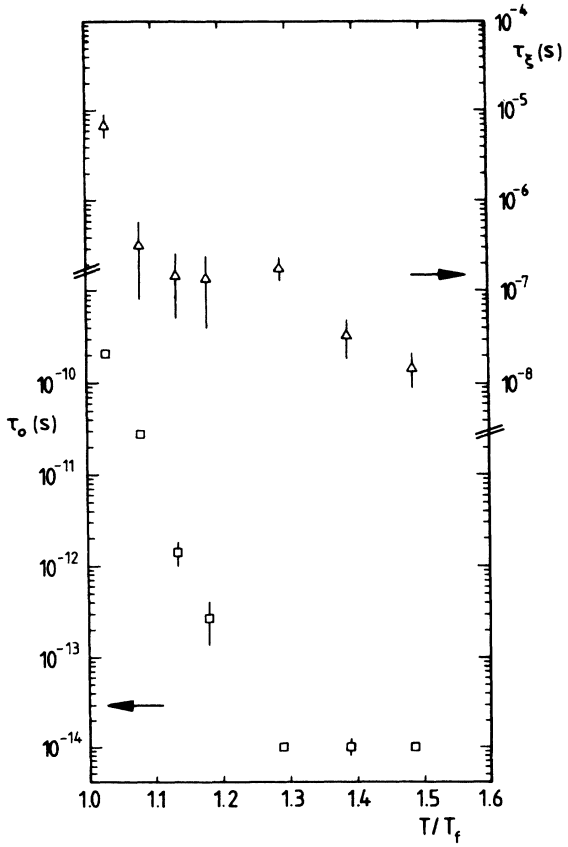

FIG. 7. Temperature dependence of the upper and lower limits τ_ξ (triangles) and τ_0 (squares) of the correlation time spectrum for *Cu*Mn(1.21 at. %) resulting from the fit strategy in Fig. 6(b).

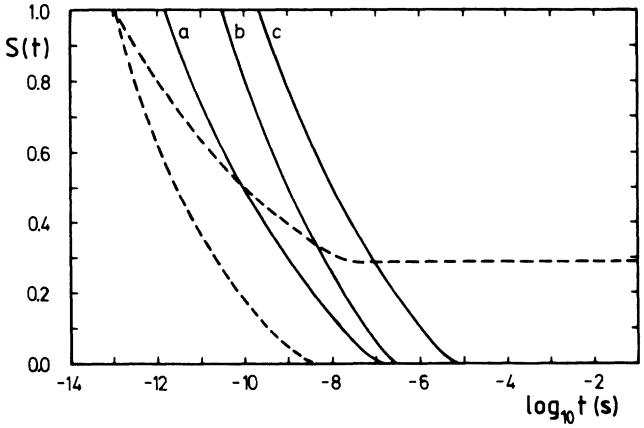

FIG. 8. Comparison of the spin autocorrelation function $S(t)$ for *Cu*Mn(1 at. %) from the neutron and χ_{ac} results in Fig. 3 (dashed lines) to the averaged local-field autocorrelation function $S_H(t)$ calculated for *Cu*Mn(1.21 at. %) using Eq. (6) with the μSR data from Fig. 7 [solid lines, $T/T_f=$ (a) 1.13; (b) 1.08; (c) 1.03].

The discrepancy becomes even more severe below T_f,[83] where the fractal cluster model predicts the decrease of the characteristic correlation time τ_ξ with decreasing temperature. For $\tau_\xi < a_0^{-1}$ follows the existence of two phases with extremely different correlation times: a totally frozen phase ($\tau=\infty$) corresponds to the infinite cluster, while the remaining small clusters generate a "paramagnetic" phase with fast fluctuating local fields, which has never been observed below $0.8T_f$.[8,84,85]

Given the fractal cluster model, we are left with the somewhat puzzling result that the spatial structure of the local-field dynamics as measured by μSR bears little or no relation to the assumed spatial configuration of the spin clusters.

VI. SPATIALLY HOMOGENEOUS LOCAL-FIELD DYNAMICS

A. The relaxation function for the muon spin

We now turn to the opposite viewpoint and assume that the local-field autocorrelation $S_H(t)$ does not vary with the muon site. From the fractal cluster model [Eq. (7)] we expect $S_H(t)$ to have the approximate form

$$S_H(t)\approx q+(1-q)S_d(t)\ , \tag{18}$$

where $S_d(t)$ follows a power law in time [Eqs. (6)and (8)] and q denotes the order parameter of the fractal cluster model [Eq. (4)].

To calculate the corresponding muon-spin-relaxation function, we will reconcile the ansatz of Eq. (18) with ideas already developed by Uemura[68,71,80] and Heffner and MacLaughlin.[51] The basic idea of Uemura is to decompose the local magnetic field into a static part H_s and a rapidly fluctuating dynamic part H_d, which serve as independent relaxation sources for the muon spin. Their amplitudes are Gaussian distributed with respective widths Δ_s and Δ_d. The total amplitude is then also Gaussian distributed with width

$$\Delta=(\Delta_s^2+\Delta_d^2)^{1/2} . \tag{19}$$

The relaxation functions corresponding to the two parts are taken as the limiting cases of the Gaussian strong collision model, i.e., for the static part we have

$$G_s^{\rm loc}(t,\Delta_s)=\tfrac{1}{3}+\tfrac{2}{3}(1-\Delta_s^2t^2)\exp(-\Delta_s^2t^2/2) \tag{20}$$

and for the dynamic part

$$G_d^{\rm loc}(t,\Delta_d,\tau)=\exp(-2\Delta_d^2\tau t) . \tag{21}$$

Here the autocorrelation for the dynamic part is assumed to be exponential and Eq. (21) requires the condition for rapid fluctuations $\Delta_d\tau\ll 1$ to be valid.

Uemura calculated the total autocorrelation for the superimposed fields as

$$S_H(t)=\frac{\Delta_s^2}{\Delta^2}+\frac{\Delta_d^2}{\Delta^2}\exp(-t/\tau) . \tag{22}$$

If we define the quantity $q_H=\Delta_s^2/\Delta^2$, Eq. (22) looks already similar to Eq. (18). Uemura[68,71,80] identified q_H with the well-known Edwards-Anderson order parameter $q_{\rm EA}$,[20] which is defined as averaged spin autocorrelation in the limit of infinite times. However, this identification is by no means self-evident: in μSR measurements the notion of a "static" field is clearly connected to the muons time window, i.e., the field appears static, if $\Delta_s\tau_s\gg 1$, where τ_s is the correlation time of the static field, which might be of order 10^{-5} s. From the probability distribution $p(\tau)$ of the fractal cluster model (Fig. 1) we can argue that the fraction of correlation times exceeding the reciprocal static linewidth will contribute to this static part, even if τ_ξ has not diverged, and consequently the order parameter q of the fractal cluster model is zero. As we shall see below, q_H turns out to be finite at and slightly above T_f.

Replacing the exponential in Eq. (22) by the approximate power law $S_d(t)$ [Eqs. (6) and (8)], we get an ansatz, which describes the local-field dynamics *effectively* probed by the muon:

$$S_H(t)=q_H+(1-q_H)S_d(t) \quad \text{with } q_H=\Delta_s^2/\Delta^2 . \tag{23}$$

This form is not only suggested by the fractal cluster model, but also removes inconsistencies in the interpretations of longitudinal-field measurements (compare Refs. 82, 86, and 87).

Concerning the validity of Eq. (21) we invoke an argument given by Heffner and MacLaughlin:[51] as long as the fluctuations are rapid, the spin-relaxation function $G_d(t)$ is not sensitive to the functional form of the autocorrelation $S_d(t)$,[73] and the correlation time τ is replaced by an effective correlation time

$$\tau_{\rm eff}=\int_0^\infty S_d(t)dt . \tag{24}$$

To calculate the total muon-spin-relaxation function we have to take the product of Eqs. (20) and (21), express Δ_s^2 and Δ_d^2 as functions of Δ^2, and perform the configuration average by integrating over the distribution $\rho(\Delta)$ [Eq. (13)]. But in doing so we only take into account the magnetic fields generated by the impurity moments. For the system *Cu*Mn, Uemura *et al.*[80] treated the fields from the Cu nuclear dipoles in the way discussed in Sec. IV. This may cause difficulties in the immediate vicinity of T_f, where the static fields from impurity moments and Cu nuclear dipoles can be of comparable amplitude. We finally remark here, that the effect of the latter can be taken into account exactly on the level of Uemura's calculation scheme: In the case of *Cu*Mn the Gaussian distribution describing the static part of the local field is a convolution of two independent Gaussian distributions with the respective widths Δ_s and $\sigma_{\rm Cu}$. Consequently we replace Δ_s^2 by $\Delta_s^2+\sigma_{\rm Cu}^2$ in Eq. (20). Performing the calculation, we arrive at the final formula for the muon-spin-relaxation function corresponding to the assumption of spatially homogeneous local-field dynamics:

$$\begin{aligned} G(t)=&\tfrac{1}{3}\exp[-(\lambda_d t)^{1/2}] \\ &+\tfrac{2}{3}\left[1-\sigma_{\rm Cu}^2t^2-\frac{a_s^2t^2}{(a_s^2t^2+\lambda_d t)^{1/2}}\right] \\ &\times\exp[-\sigma_{\rm Cu}^2t^2/2-(a_s^2t^2+\lambda_d t)^{1/2}] . \end{aligned} \tag{25}$$

Since the quantity $q_H=\Delta_s^2/\Delta^2$ is explicitly assumed to be site independent, i.e., independent of Δ, it is not affected by the configuration average. Here only the Gaussian linewidths are replaced by the corresponding Lorentzian ones and we have the additional relations

$$a_s^2=q_Ha_0^2, \quad a_d^2=(1-q_H)a_0^2, \quad \lambda_d=4a_d^2\tau_{\rm eff} , \tag{26}$$

where a_0 denotes the static Lorentzian linewidth in the limit $T\to 0$ [see Eq. (28)]. Finally the condition for rapid fluctuations of the dynamic part becomes

$$a_d\tau_{\rm eff}\ll 1 . \tag{27}$$

Equation (25) includes various limits already discussed in the text. For example, for $q_H=0$, corresponding to a superposition of static nuclear dipole fields and rapidly and isotropically fluctuating Mn impurity fields, Eq. (25) reduces to the product of the exponential-root law [Eq. (9)] and the Kubo-Toyabe function [Eq. (12)]. If q_H (and consequently a_s) is finite, we may visualize the local field as fluctuating rapidly in a finite solid angle, where the symmetry axis of the latter varies randomly with the muon site. As it is also clear from the foregoing, this general physical picture has been used by other μSR investigators before, but we have now reconciled different aspects of their interpretation and will relate the results to the fractal cluster model of MBC below.

B. Data evaluation: static linewidth and dynamic relaxation rate

We have analyzed new data for six different polycrystalline spin-glass samples out of the two systems *Cu*Mn and *Au*Mn with the relaxation function Eq. (25). Their characteristic properties are given in Table II together with the symbols used in the following figures.

Equation (25) permits a very good overall description of the measured data, except for the *Cu*Mn system, where some deviations occur in a small temperature interval around T_f. We comment on them in Sec. VII. Fit examples have already been given in Figs. 4 and 5 in Sec. IV.

Figures 9(a) and 9(b) show the scaled static linewidth a_s/c separately for each system as a function of the reduced temperature T/T_f. The limiting values for $T\rightarrow 0$ have been calculated by Mikaelyan and Smilga[67] for the case of pure dipolar coupling as

$$a_0(T=0)=4.5406 n_a c \gamma_\mu g_{\text{eff}} \mu_B S \tag{28}$$

(see also Ref. 88). Here n_a denotes the host site density ($=4/a^3$, where a is the fcc lattice constant), c is the impurity concentration, γ_μ the gyromagnetic ratio for the muon, and g_{eff} and S the effective g value and spin for the impurity moment. Equation (28) may be written as $a_0=Kc$, where the system dependent constant K is given by[89]

$$\begin{aligned} K(Cu\text{Mn}) &= 13.05\ \mu\text{s}^{-1}/\text{at. \%}\ , \\ K(Au\text{Mn}) &= 9.84\ \mu\text{s}^{-1}/\text{at. \%}\ . \end{aligned} \tag{29}$$

To compare both systems, we scaled a_s using the respective values for a_0 [Fig. 9(c)]. To a very good accuracy the temperature dependence of a_s/a_0 is common to all six samples. It is important to note that the static linewidth is *finite* at T_f, where $a_s/a_0\approx 0.2$, contrary to the results reported by Uemura *et al.*[71,80] It drops to unmeasurable values above approximately $1.05T_f$.

The dynamic relaxation rate λ_d depends on temperature through both the amplitude $a_d(T)$ of the dynamic part of the local field and its effective correlation time τ_{eff}. Rewriting Eqs. (26) we get

$$\lambda_d = 4a_0^2(1-q_H)\tau_{\text{eff}} = 4c^2K^2(1-q_H)\tau_{\text{eff}}\ , \tag{30}$$

where the constant K is given in Eq. (29).

TABLE II. Characteristics of the polycrystalline spin glasses investigated in the μSR measurements (see also Table IV). The last column gives the respective symbols used in the following figures.

Sample	Concentration (at. %)	T_f (K)	Symbol
*Cu*Mn(0.65)	0.65	7.6	○
*Cu*Mn(1.03)	1.03	10.62	□
*Cu*Mn(1.21)	1.21	11.3	△
*Au*Mn(0.84)*A*	0.84	4.05	●
*Au*Mn(0.84)*B*	0.84	4.19	■
*Au*Mn(1.15)	1.15	5.36	▲

Since from Fig. 9(c) we can regard $q_H(T)$ as a unique function of temperature in all samples (see also Fig. 13), differences in the temperature dependence of λ_d directly bear on differences in the effective correlation times. As

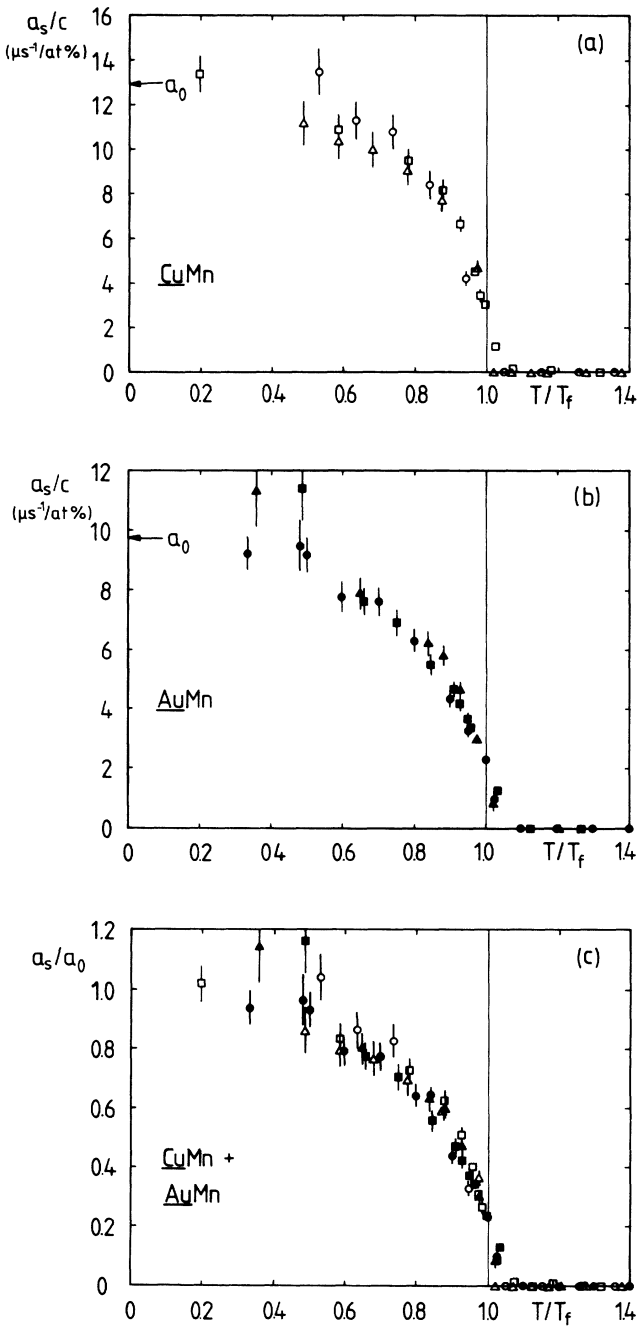

FIG. 9. Scaled static linewidth a_s/c for (a) three different polycrystalline *Cu*Mn spin glasses and (b) three different *Au*Mn spin glasses as functions of the reduced temperature T/T_f (for symbols see Table II). In the limit $T\rightarrow 0$ the data can be extrapolated for each system to the respective value a_0 calculated from the Mikaelyan-Smilga theory for pure dipolar coupling [Eq. (29)]. The scaled linewidths a_s/a_0 show (c) the same temperature dependence in all six samples.

MacLaughlin *et al.*[86] pointed out, all fluctuation frequencies ν in spin glasses should scale as the average exchange interaction $J_{av}=k_B T_f$ and consequently $\tau_{eff}=1/\nu_{eff}$ should be proportional to $1/T_f$. We can check this relation by plotting the scaled relaxation rate $\lambda_d T_f/c^2$ versus the reduced temperature T/T_f, which is done in Fig. 10(a).[90]

Contrary, Uemura *et al.*[80] found the same *absolute* values for τ_{eff} as a function of temperature in the spin-glass systems *Cu*Mn and *Au*Fe. Then the appropriate quantity for comparison is λ_d/c^2, which is shown in Fig. 10(b). Figures 10(a) and 10(b) clearly suggest that in our samples τ_{eff} varies as $1/T_f$.[91] It seems that in Ref. 80 this relation is broken by *Cu*Mn samples with relatively large concentrations (3 and 5 at. %), where the scaling laws are not expected to be valid.[92]

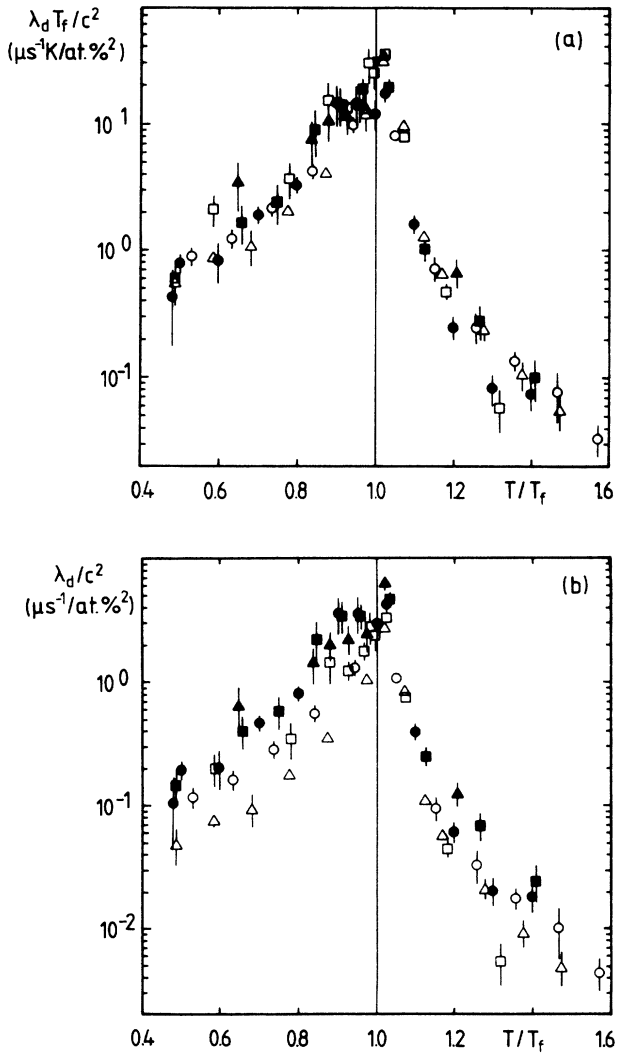

FIG. 10. Dynamic relaxation rate λ_d for the six spin-glass samples from Table II scaled in different ways to test for the T_f dependence of the effective correlation time τ_{eff}. The much better scaling in (a) suggests that τ_{eff} is proportional to $1/T_f$ (see text).

C. Data evaluation: aspects of a phase transition

We now ask whether the parameters from the preceding section apart from their scaling behavior reflect phase-transition properties. As we have already seen in Fig. 9, the static linewidth a_s is finite at T_f. Consequently we cannot interpret $q_H=a_s^2/a_0^2$ as an order parameter in the vicinity of T_f.

Another problem arises from the temperature dependence of λ_d above T_f. Here we have $a_s=0$ and the steep increase of λ_d directly reflects the temperature dependence of τ_{eff}. From the fractal cluster model the effective correlation time can be derived from Eqs. (24), (5), and (2) as

$$\tau_{eff}=\int_0^\infty S_d(t)dt=\int_{\tau_0}^{\tau_\xi}\tau p(\tau)d\ln\tau$$
$$=\frac{1}{C}\frac{\tau_0}{\delta x-1}[(\tau_\xi/\tau_0)^{1-1/(\delta x)}-1]\,, \tag{31}$$

with the normalization constant C given by Eq. (3).

Equation (31) predicts a divergence of τ_{eff} with an effective exponent w:

$$\tau_{eff}\propto\tau_\xi^{1-1/(\delta x)}\propto\epsilon^{-\nu z(1-1/\delta x)}=:\epsilon^{-w}\,, \tag{32}$$

where νz is the dynamical critical exponent, which controls the divergence of τ_ξ at T_f.[93]

Figure 11 shows the scaled effective correlation time $\tau_{eff}T_f$ versus the reduced temperature $\epsilon=(T-T_f)/T_f$. For $\epsilon>0.05$ the data may be represented by the power law Eq. (32) with $w=2.6\pm0.3$, which agrees very well with values given by Uemura *et al.*[80] However, inserting $\delta x\approx10$ from the analysis of the neutron and χ_{ac} data, we get $\nu z=2.9\pm0.3$ which clearly deviates from the larger values $\nu z\approx7$ obtained from dynamical scaling for several

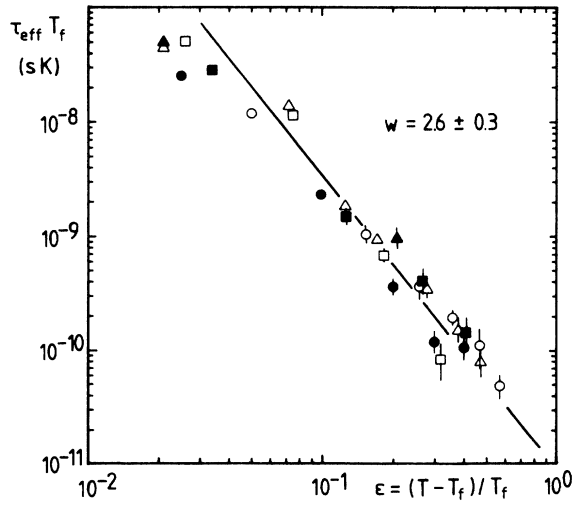

FIG. 11. Scaled effective correlation time $\tau_{eff}T_f$ as a function of the reduced temperature $\epsilon=(T-T_f)/T_f$ above the freezing temperature for the six *Cu*Mn and *Au*Mn samples. The straight line corresponds to a power law $\tau_{eff}T_f\propto\epsilon^{-w}$ with an exponent $w=2.6\pm0.3$.

spin-glass systems.[21,23–25] We could argue that temperatures $\epsilon > 0.05$ do not correspond to the critical region and the correct exponents have to be determined from temperatures much closer to T_f.[94] But in Fig. 11 the value of w *decreases* for smaller ϵ and an even more pronounced curvature has been reported by Uemura *et al.*[80]

We believe that we must take into account the finite time window of the μSR method here. This can be done approximately in the frame of the fractal cluster model by assuming that correlation times τ larger than the reciprocal static linewidth $1/a_0$ do not contribute to the effective correlation time τ_{eff}, but to the static part of the local field and hence lead to finite values of q_H already above T_f. If the characteristic correlation time τ_ξ of the fractal cluster model exceeds $1/a_0$, we have to replace τ_ξ in the integral of Eq. (31) by $1/a_0$ and in addition we get q_H as

$$q_H = \int_{1/a_0}^{\tau_\xi} p(\tau) d \ln\tau = \frac{1}{C}[(a_0\tau_0)^{1/(\delta x)} - (\tau_0/\tau_\xi)^{1/(\delta x)}] \quad \text{if } \tau_\xi > a_0^{-1} . \tag{33}$$

It follows that the quantities q_H and τ_{eff}, as measured by μSR, will reflect the corresponding critical quantities q and τ_ξ of the fractal cluster model only if $\tau_\xi < 1/a_0$, that is, outside a certain temperature interval around T_f. These considerations also permit the comparison of the μSR results to the analysis of neutron and χ_{ac} data in Sec. III.

D. Comparison to the neutron and χ_{ac} data

Using Eqs. (31) and (33) we have computed from the model parameters in Table I the quantities τ_{eff}^N and q_H^N in Table III (the superscript N refers to the neutron data), which should now correspond to the μSR results. The most remarkable feature of the data in Table III is the *decrease* of τ_{eff}^N with decreasing temperature below T_f. Although the experimental methods are entirely distinct, the same qualitative temperature dependence is found in the μSR data, when τ_{eff} is calculated via Eq. (30). Figure 12 shows the scaled correlation time $\tau_{\text{eff}} T_f$ together with the corresponding values for $\tau_{\text{eff}}^N T_f$ from Table III.

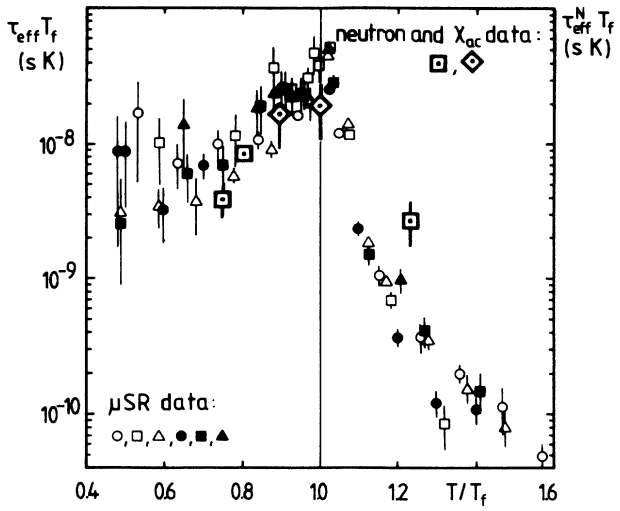

FIG. 12. Temperature dependence of the effective local-field correlation time $\tau_{\text{eff}} T_f$ calculated from the μSR data in Figs. 9 and 10 via Eq. (30) (small symbols, see Table II). Large symbols denote the effective correlation time $\tau_{\text{eff}}^N T_f$, which is computed for the μSR time window (see text) from the results of the neutron and χ_{ac} data analysis in Sec. III (Tables I and III: ⊡, $\tau_\xi < 1/a_0$; ◇, $\tau_\xi > 1/a_0$). In both cases the effective correlation time *decreases* with decreasing temperature for $T < T_f$. Below about $T/T_f = 0.6$ the temperature dependence becomes obscured by the large scatter.

The unusual behavior of τ_{eff} below T_f is interpreted within the fractal cluster model as the growth of the infinite cluster, which always incorporates the *largest* remaining clusters, thereby leaving smaller clusters with smaller correlation times free to rotate (see also Fig. 1).[95]

We emphasize here that the decrease of τ_{eff} in the μSR data is not anticipated by the use of the relaxation function Eq. (25). The effective correlation time is calculated

TABLE III. Effective correlation time τ_{eff}^N and (effective) order parameter q_H^N derived from the analysis of neutron and χ_{ac} data in Sec. III (Table I). The limited time window of the μSR method was taken into account in the computation (for the details see text).

Symbol in Figs. 2 and 3	T/T_f	τ_{eff}^N (s)	$\tau_{\text{eff}}^N T_f$ (s K)	q_H^N
*Cu*Mn(1 at. %)		$T_f = 9.9$ K	$1/a_0 = 8\times10^{-8}$ s	
a	0.8	$(8.6\pm0.4)\times10^{-10}$	$(8.6\pm0.4)\times10^{-9}$	0.32±0.01
b	1.23	$(2.6\pm0.8)\times10^{-10}$	$(2.6\pm0.8)\times10^{-9}$	
*Cu*Mn(3 at. %)		$T_f = 20$ K	$1/a_0 = 2.7\times10^{-8}$ s	
a	0.25	$(3.8\pm1)\times10^{-12}$	$(8\pm2)\times10^{-11}$	0.88±0.02
b	0.75	$(2.0\pm0.6)\times10^{-10}$	$(4.0\pm1.2)\times10^{-9}$	0.49±0.01
c	0.9	$(8.5\pm0.4)\times10^{-10}$	$(1.7\pm0.8)\times10^{-8}$	0.33±0.07
d	1.0	$(9.9\pm0.4)\times10^{-10}$	$(2.0\pm0.8)\times10^{-8}$	0.25±0.04

from the two parameters a_s and λ_d [see Eqs. (26) and (30)], which are independent below $0.8T_f$ since a_s is determined by the initial slope of $G(t)$ at short times and λ_d is controlled by the decay of the 1/3 tail (see Figs. 4 and 5). The decrease of τ_{eff} is also insensitive to the choice of a_0 in the temperature range $0.4T_f - 1.0T_f$. Here larger values of τ_{eff} would require smaller values of a_0 which are hardly consistent with Figs. 9(a) and 9(b). Below $0.4T_f$ the errors in the computation of the factor $1-q_H$ in Eq. (30) become so large that a 10% change of a_0 causes τ_{eff} to vary by more than 2 orders of magnitude. At the lowest temperature $T=0.25T_f$ in Table III also the τ_{eff}^N value which is much smaller than the μSR data seems to be quite uncertain (c.f. the corresponding value δx in Table I).

From τ_{eff} we calculate a maximum value of the parameter $a_d\tau_{\text{eff}} \approx 0.1$ in the vicinity of T_f, which validates the condition for rapid fluctuations of the dynamic part of the local field [Eq. (27)].

Finally Fig. 13 shows the comparison of $q_H = a_s^2/a_0^2$ and the values for q_H^N from Table III. The agreement is very good below T_f, but at T_f the value deduced from the time window considerations is too large. However, we should keep in mind that there are no adjustable parameters for the comparison in Figs. 12 and 13 and we have analyzed results from completely different methods applied to different samples. If we neglect the time window, the figures show unreasonably large discrepancies and the interpretation of the temperature dependence of τ_{eff} above T_f becomes considerably more difficult.

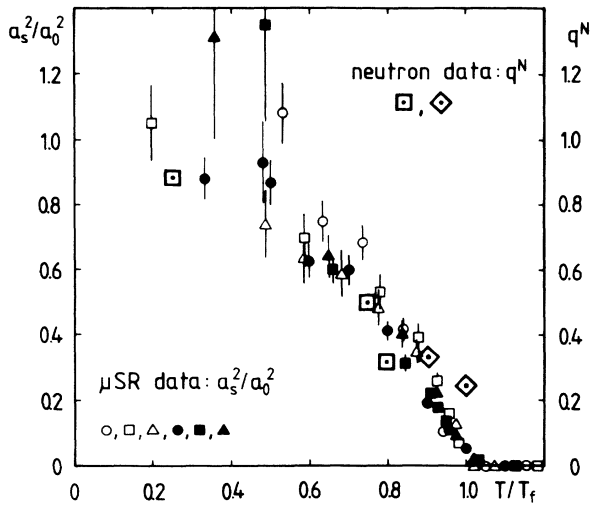

FIG. 13. Temperature dependence of the quantity $q_H = a_s^2/a_0^2$ calculated from the μSR data in Fig. 9(c) in comparison to the corresponding quantity q_H^N, which is computed from the results of Sec. III (Tables I and III) according to the μSR time window considerations discussed in the text (□, $\tau_\xi < 1/a_0$; ◇, $\tau_\xi > 1/a_0$).

VII. LIMITATIONS FOR THE MODEL OF HOMOGENEOUS LOCAL-FIELD DYNAMICS

The results of Sec. VI are clearly at variance with our earlier interpretation of μSR measurements on *Cu*Mn single crystals.[8,84,85] These former measurements were analyzed in terms of a two phase model, which was clearly superior to the homogeneous freezing model of Eq. (25). But subsequent measurements on polycrystalline samples showed that the "inhomogeneous" two phase model (which is different to the model discussed in Sec. V) and the "homogeneous" model from Sec. VI could be equally well fitted to the data.

To clarify this difference, we prepared a large number of samples, which were subjected to different thermal and mechanical pretreatments. Extensive sample characterization as described below singled out the large-scale homogeneity (on cm distances) as a major problem in the single crystals.

Information about homogeneity were obtained by three methods: chemical analysis with atomic emission spectroscopy, microprobe analysis, and ac susceptibility measurements. Multiple determination of the freezing temperature T_f for different cutoff pieces provides a sensitive and convenient method to check the homogeneity, since for impurity concentrations around 1 at. % the freezing temperature varies approximately linearly with concentration and can be measured with a relative accuracy better than 0.5%. Like T_f measurements the chemical analysis probes concentration variations on mm and cm distances, whereas microprobe analysis yields corresponding information for length scales between 1 and 50 μm and is therefore sensitive below typical grain sizes in polycrystalline material.

In single crystals we found that the Mn concentration may vary occasionally along the axis of crystal growth up to 10% from one end to the other. The crystals were originally grown in the form of long slim cylinders (4 mm diameter, 100 mm length), then cut into shorter parts and glued together. Our judgement of the spin-glass quality was based on the sharpness of the ac cusp and had to fail since only one small cutoff piece was measured for each sample. Later the chemical analysis gave a moderate variation of approximately 5% between several parts of the μSR samples.

In polycrystalline material the homogeneity did already depend on the way in which the raw alloy was prepared. In most cases the constituents were alloyed by induction heating in Al_2O_3 crucibles under high vacuum ($< 10^{-5}$ Torr) and then poured into an ingot mold. The worst homogeneity occurred, when the alloy was allowed to solidify slowly in the crucible which resulted in relatively large grains. Microprobe analysis revealed concentration inhomogeneities up to 16% in these cases, which were hardly affected by annealing. The best results were achieved by swaging the ingots to less than 40% of their original diameter followed by annealing at temperatures around 900 °C. This combination of severe cold working with subsequent homogenization annealing has also proved to be successful for other alloys.[96,97]

The six polycrystalline samples used in the μSR mea-

surements in Sec. VI are characterized in Table IV. For the samples *Cu*Mn(1.03 at. %) and *Cu*Mn(1.21 at. %) no concentration variation could be detected within experimental resolution. Here the relative accuracies of the methods are given as upper limits. For the sample *Cu*Mn(0.65 at. %) only a marginal difference was found. The homogenization procedure did work for the *Au*Mn(0.84 at. %)*A* sample also, but surprisingly not as well for the two others, for reasons which are unclear at present. However, the variations are still comparable to those reported by other authors,[6,80,98] whereas our results for the *Cu*Mn system are clearly better.

The homogeneity did not depend on the way the samples were cooled down from the annealing temperature, i.e., no differences were found between slowly cooled and quenched samples. In this context we consider the annealing, which necessarily precedes the quenching, to be more important than the quench itself.[99] The latter affects the atomic short-range order,[1] but it is not clear whether this should show up in a μSR measurement.

Finally the two systems seem to differ somewhat in detail, because for *Cu*Mn deviations from the model of homogeneous local-field dynamics occurred in a small temperature interval $0.95 < T/T_f < 1.02$ (Fig. 14), whereas no deviations were found in the *Au*Mn samples in spite of their larger inhomogeneity. The maximum normalized χ^2 for the model function Eq. (25) found in *Cu*Mn(1.03 at. %) at T_f reduces from the value 1.6 to 1.02 if an inhomogeneous model similar to that of Refs. 8, 84, and 85 is fitted to the data. We cannot rule out residual inhomogeneities as the origin of these deviations, because microprobe analysis only guarantees an upper limit of 2.5% (see Table IV), but we are convinced that the preparation can hardly be improved. In this sense we consider spatial inhomogeneous freezing as incident to "real life" *Cu*Mn spin glasses.

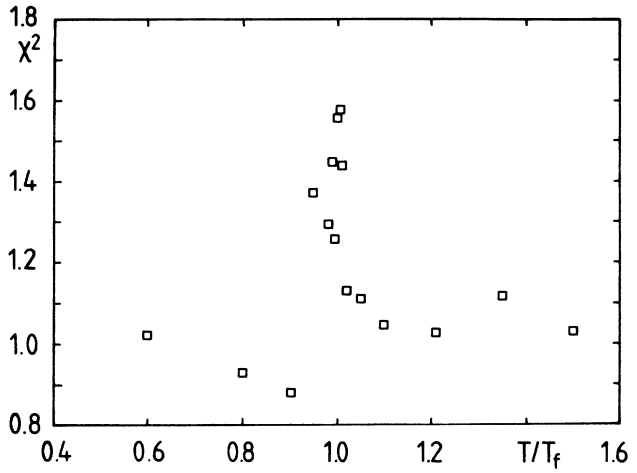

FIG. 14. Data evaluation for the *Cu*Mn(1.03 at. %) sample with the model of homogeneous local-field dynamics [Eq. (25)]. Shown are values for normalized χ^2 vs the reduced temperature T/T_f. The measured relaxation function deviates from the model in the vicinity of T_f ($0.95 < T/T_f < 1.02$) which is indicated by the significant increase of χ^2.

VIII. SUMMARY AND DISCUSSION

We have presented a comparative analysis of neutron, zero-field μSR, and ac susceptibility data for the spin-glass systems *Cu*Mn and *Au*Mn in the frame of the critical fractal cluster model of Malozemoff, Barbara, and Continentino.[46,47]

For our purposes we reformulated the model in terms of a probability distribution of spin-correlation times $p(\tau)$. The distribution is controlled by three model pa-

TABLE IV. Characteristic properties of the six polycrystalline spin-glass samples investigated in this work. Concentration c and freezing temperature T_f are given as average values in cases of multiple determination. The column homogeneity then should be read as approximate standard deviations to these values.

Sample	Annealing Temp. (°C)	Annealing Time (h)	c (at. %)	T_f (K)	Relative homogeneity (%)	Determined by
*Cu*Mn(0.65)	900	6	0.65	7.6	1	Chem. analysis
					2	multiple T_f
*Cu*Mn(1.03)	950	10	1.03	10.62	0.5	Chem. analysis
					0.5	multiple T_f
					2.5	microprobe
*Cu*Mn(1.21)	900	6	1.21	11.3	1	Chem. analysis
					2.5	microprobe
*Au*Mn(0.84)*A*	950	12	0.84	4.05	1	Chem. analysis
					1	multiple T_f
*Au*Mn(0.84)*B*	930	10	0.84[a]	4.19	2	multiple T_f
*Au*Mn(1.15)	930	10	1.15[a]	5.36	4	multiple T_f

[a]Nominal concentration.

rameters, the lower and upper limits τ_0 and τ_ξ of the correlation time spectrum, and the critical exponent $1/(\delta x)$. Suitable approximations with respect to the time windows of μSR and NSE allowed to calculate the spin-autocorrelation function

$$S(t)=q+(1-q)S_d(t)\ ,$$

where $q=(\tau_0/\tau_\xi)^{1/(\delta x)}$ denotes the order parameter of the model and $S_d(t)$ approximately follows a power law $S_d(t)\propto(t/\tau_0)^{1/(\delta x)}$. The analysis of neutron and ac susceptibility data of Mezei and Murani[3-5] gave the model parameters for a few reduced temperatures T/T_f, which then enabled a quantitative comparison to the μSR results.

The access to impurity spin dynamics through μSR is more indirect, since the muon is a localized probe and sensitive to the fluctuations of the magnetic field at its site. Therefore we had to characterize in a first step the dynamics of this local field, which cannot be directly inferred from the fractal cluster model. In a second step we assumed that the field autocorrelation $S_H(t)$ averaged over all muon sites can be compared with the spin autocorrelation $S(t)$. We considered two extreme cases for the local-field dynamics.

The assumption that contributions from a given cluster dominate the local magnetic field at all muon sites within the volume of that cluster has led to the model of spatially inhomogeneous local-field dynamics. This model turned out to be inapplicable below T_f. Above T_f the resulting temperature dependence of the averaged local-field autocorrelation $S_H(t)$ clearly disagreed with the analysis of the neutron and χ_{ac} data.

A spatially homogeneous model for the local-field dynamics followed from the assumption that the local magnetic field is essentially a superposition of many contributions from impurity spins fluctuating with different correlation times. In view of the fractal cluster model this results from interpenetrating clusters with porous and fractal geometry in addition to the long-ranged dipolar coupling between muon and impurity spin. To evaluate the data we have linked the fractal cluster model to Uemura's model of coexisting static and dynamic fields[68,71,80] and Heffner's and MacLaughlin's interpretation of the effective correlation time τ_{eff} caused by a nonexponential autocorrelation function of the dynamic part.[51] A large amount of μSR data for six polycrystalline spin glasses belonging to the two systems *Cu*Mn and *Au*Mn allowed a conclusive scaling analysis of the model parameters static linewidth a_s and dynamic relaxation rate λ_d. The scaled static linewidth a_s/a_0 and the scaled effective correlation time $\tau_{eff}T_f$ of the dynamic part of the local field are to a very good accuracy universal functions of the reduced temperature T/T_f in all our samples.

The quantities $q_H=(a_s/a_0)^2$ and τ_{eff} play the same role for the averaged local-field autocorrelation $S_H(t)$ as do the order parameter q and the characteristic correlation time τ_ξ for the spin autocorrelation $S(t)$ in the frame of the fractal cluster model. However, q_H and τ_{eff} cannot directly be interpreted as critical parameters in a phase transition picture because of two reasons. (1) The static linewidth a_s/a_0 is finite at T_f. (2) The temperature dependence of τ_{eff} above T_f can be roughly described by a power law $\tau_{eff}\propto(T/T_f-1)^{-w}$ with an exponent $w\approx2.6$. But this value for the effective exponent $w=\nu z(1-1/\delta x)=\nu z-\beta$ leads to appreciable discrepancies to the results of other experiments, which probe long-time scales. These values are compared in Table V.

As we have discussed, this problem can probably be resolved by taking into account the finite time window of the μSR method. Here the reciprocal static linewidth $1/a_0$ sets a time scale, which divides the correlation time spectrum into a dynamic and a static part. As a result the behavior of the quantities q_H and τ_{eff} as measured by μSR reflects the temperature dependence of the critical parameters q and τ_ξ only outside a certain temperature interval around T_f. The time window considerations led to a reasonable agreement between μSR results and the analysis of neutron and χ_{ac} data in Sec. III. However, a precise investigation of identical samples by μSR and methods such as relaxation of thermoremanence or dynamic susceptibility studies at ultralow frequencies would be desirable to confirm that the critical temperature re-

TABLE V. Values for several critical exponents determined from scaling analyses of the experimental results. For the 3*d* short-range Ising model and mean-field theory (MFT) we have related δx to the temperature-dependent exponent γ ($\delta x=1/\gamma$) (Ref. 36), which controls the time decay of the spin autocorrelation $S(t)\propto t^{-\gamma}$.

	Parameter			
νz	β	$\delta x=\nu z/\beta$	System	Reference
7±0.6	0.9±0.2	7.8±2	AgMn	24,25
8.2±1	0.38±0.04	21±6	FeNiPBAl	23
8.2±0.5			EuSrS	21
7.2±1	(≈0.5)	$1/\gamma\approx15$ at T_f	num. 3*d* short-range Ising	42
2	1	$4\geq1/\gamma\geq2$ (=2 at T_f)	dynamic MFT	35,36
2.9–3.2		if $\delta x\approx10$	CuMn	μSR: 80
≈2.9		if $\delta x\approx10$	CuMn	μSR: this work

gion is indeed inaccessible to μSR.

Given the above restrictions, our results are consistent with the existence of a phase transition in the spin-glass systems *Cu*Mn and *Au*Mn, but we cannot provide direct evidence from our analysis. We only note here that the large values $\delta x \geq 10$ obtained for *Cu*Mn in Sec. III are in better agreement with recent experimental determinations than with mean-field theory (see Table V).

The most remarkable prediction of the fractal cluster model is that of a temperature-dependent upper limit τ_ξ of the correlation time spectrum, which diverges at T_f and decreases again if the temperature is lowered below T_f. Qualitatively the corresponding behavior was found for the effective correlation time τ_{eff} of the local magnetic field.

ACKNOWLEDGMENTS

A part of this work has emerged from a long and fruitful collaboration with the μSR group at the Eidgenössische Technische Hochschule Zürich. We are deeply indebted to Dr. A. Schenck, Dr. F. N. Gygax, E. Lippelt, B. Hitti, and P. Birrer for numerous stimulating discussions, invaluable encouragement during the experiments, and their kind hospitality. The authors also wish to thank the staff at the Paul Scherrer Institute in Villigen, Switzerland (the former Swiss Institute for Nuclear Research) for their kind support. Further we would like to thank Professor J. A. Mydosh and C. Snel at the Kamerlingh Onnes Laboratories in Leiden, Netherlands, where the *Au*Mn(0.84 at. %)*A* sample has been prepared, and Dr. Zachmann from the Institute for Geology at the Technische Universität Braunschweig for his collaboration in the chemical analysis. The help of S. Kahl from our own institute, who performed parts of the susceptibility measurements and chemical analysis, is gratefully acknowledged. One of us (H.P.) has also benefitted very much from discussions with Professor D. E. MacLaughlin (University of California, Riverside). This work has received financial support from the Bundesministerium für Forschung und Technologie, Bonn, Federal Republic of Germany.

*Present address: Physikalisches Institut, TU Clausthal, Leibnizstrasse 4, 3392 Clausthal-Zellerfeld, Federal Republic of Germany.

[1]The experimental situation in spin glasses has been repeatedly reviewed by J. A. Mydosh, J. Magn. Magn. Mater. 7, 237 (1978); in *Lecture Notes in Physics* (Springer, Heidelberg, 1981), Vol. 149, p. 87; in *Lecture Notes in Physics* (Springer, Heidelberg, 1983), Vol. 192, p. 38; Hyperfine Interact. **31**, 347 (1986); see also the compilation by K. H. Fischer, Phys. Status Solidi B **116**, 357 (1983).

[2]V. Cannella, J. A. Mydosh, and J. I. Budnick, J. Appl. Phys. **42**, 1689 (1971).

[3]F. Mezei and A. P. Murani, J. Magn. Magn. Mater. **14**, 211 (1979).

[4]F. Mezei, J. Appl. Phys. **53**, 7654 (1982); J. Magn. Magn. Mater. **31-34**, 1327 (1983).

[5]A. P. Murani, J. Phys. F **15**, 417 (1985).

[6]Y. J. Uemura, T. Yamazaki, R. S. Hayano, R. Nakai, and C. Y. Huang, Phys. Rev. Lett. **45**, 583 (1980).

[7]R. H. Heffner, M. Leon, M. E. Schillaci, D. E. MacLaughlin, and S. A. Dodds, J. Appl. Phys. **53**, 2174 (1982).

[8]K. Emmerich, F. N. Gygax, A. Hintermann, H. Pinkvos, A. Schenck, Ch. Schwink, and W. Studer, J. Magn. Magn. Mater. **31-34**, 1361 (1983).

[9]J. L. Tholence, Solid State Commun. **35**, 113 (1980).

[10]C. A. M. Mulder, A. J. van Duyneveldt, and J. A. Mydosh, Phys. Rev. B **23**, 1384 (1981).

[11]L. Lundgren, P. Svedlindh, and O. Beckmann, J. Phys. F **12**, 2663 (1982).

[12]R. V. Chamberlin, G. Mozurkewich, and R. Orbach, Phys. Rev. Lett. **52**, 867 (1984).

[13]P. Nordblad, P. Svedlindh, L. Lundgren, and L. Sandlund, Phys. Rev. B **33**, 645 (1986).

[14]M. Alba, M. Ocio, and J. Hammann, Europhys. Lett. **2**, 45 (1986).

[15]M. Ocio, H. Bouchiat, and P. Monod, J. Magn. Magn. Mater. **54-57**, 11 (1986).

[16]W. Reim, R. H. Koch, A. P. Malozemoff, M. B. Ketchen, and H. Maletta, Phys. Rev. Lett. **57**, 905 (1986).

[17]M. Alba, J. Hammann, M. Ocio, P. Refregier, and H. Bouchiat, J. Appl. Phys. **61**, 3683 (1987).

[18]P. Svedlindh, P. Nordblad, and L. Lundgren, Phys. Rev. B **37**, 2383 (1988).

[19]For a general use of spin-correlation functions see R. Kubo, J. Phys. Soc. Jpn. **12**, 570 (1957).

[20]S. F. Edwards and P. W. Anderson, J. Phys. F **5**, 965 (1975).

[21]N. Bontemps, J. Rajchenbach, R. V. Chamberlin, and R. Orbach, J. Magn. Magn. Mater. **54-57**, 1 (1986).

[22]P. Beauvillain, J. P. Renard, M. Matecki, and J. J. Prejean, Europhys. Lett. **2**, 23 (1986).

[23]P. Svedlindh, L. Lundgren, P. Nordblad, and H. S. Chen, Europhys. Lett. **3**, 243 (1987).

[24]L. P. Levy and A. T. Ogielski, Phys. Rev. Lett. **57**, 3288 (1986).

[25]L. P. Levy, Phys. Rev. B **38**, 4963 (1988).

[26]P. C. Hohenberg and B. I. Halperin, Rev. Mod. Phys. **49**, 435 (1977).

[27]I. A. Campbell, Phys. Rev. B **37**, 9800 (1988).

[28]K. Binder and A. P. Young, Phys. Rev. B **29**, 2864 (1984).

[29]A. P. Malozemoff and E. Pytte, Phys. Rev. B **34**, 6579 (1986).

[30]E. Pytte and Y. Imry, Phys. Rev. B **35**, 1465 (1987).

[31]L. Lundgren, P. Svedlindh, P. Nordblad, and O. Beckmann, Phys. Rev. Lett **51**, 911 (1983); J. Appl. Phys. **57**, 3371 (1985).

[32]P. Nordblad, P. Svedlindh, L. Lundgren, and L. Sandlund, Phys. Lett. A **120**, 475 (1987).

[33]D. S. Fisher and D. A. Huse, Phys. Rev. Lett. **56**, 1601 (1986); Phys. Rev. B **38**, 373 (1988); **38**, 386 (1988).

[34]G. J. M. Koper and H. J. Hilhorst, J. Phys. (Paris) **49**, 429 (1988).

[35]H. Sompolinski and A. Zippelius, Phys. Rev. Lett. **47**, 359 (1980); Phys. Rev. B **25**, 6860 (1982); J. Phys. C **15**, L1059 (1982).

[36]An excellent discussion of various EA models has been given by K. Binder and A. P. Young, Rev. Mod. Phys. **58**, 801 (1986).

[37]See also A. A. Abrikosov, Adv. Phys. **29**, 869 (1980); K. H. Fischer, Phys. Status Solidi B **130**, 14 (1985); D. Chowdhury and A. Mookerjee, Phys. Lett. C **114**, 1 (1984).

[38]J. A. Olive, A. P. Young, and D. Sherrington, Phys. Rev. B **34**, 6341 (1984).

[39]R. N. Bhatt and A. P. Young, Phys. Rev. B **37**, 5606 (1988).
[40]L. R. Walker and R. E. Walstedt, Phys. Rev. B **22**, 3816 (1980); J. Magn. Magn. Mater. **31-34**, 1289 (1983); R. E. Walstedt and L. R. Walker, J. Appl. Phys. **53**, 7985 (1982); R. E. Walstedt, Physica B+C **109+110B**, 1924 (1982).
[41]A. Chakrabarti and C. Dasgupta, Phys. Rev. B **36**, 793 (1987); J. Phys. C **21**, 1613 (1988).
[42]A. T. Ogielski, Phys. Rev. B **32**, 7384 (1985).
[43]M. Cyrot, Solid State Commun. **39**, 1009 (1981).
[44]A. Mookerjee and D. Chowdhury, J. Phys. F **13**, 431 (1983); D. Chowdhury and A. Mookerjee, *ibid.* **14**, 245 (1984); Physica B+C **124B**, 255 (1984).
[45]B. Barbara, A. P. Malozemoff, and Y. Imry, Phys. Rev. Lett. **47**, 1852 (1981).
[46]A. P. Malozemoff and B. Barbara, J. Appl. Phys. **57**, 3410 (1985).
[47]M. A. Continentino and A. P. Malozemoff, Phys. Rev. B **33**, 3591 (1986); **34**, 471 (1986).
[48]D. Stauffer, Phys. Rep. **54**, 1 (1979).
[49]L. Lundgren, P. Nordblad, and P. Svedlindh, Phys. Rev. B **34**, 8164 (1986).
[50]See, e.g. A. P. Murani, Solid State Commun. **33**, 433 (1980); L. E. Wenger, in *Lecture Notes in Physics* (Springer, Berlin, 1983), Vol. 192, p. 60.
[51]R. H. Heffner and D. E. MacLaughlin, Phys. Rev. B **29**, 6048 (1984).
[52]Due to the approximations made for the scaling function $f(y)$, Eqs. (6) and (7) neglect a very weak time dependence of $S(t)$ for $t > \tau_{\xi}$. We consider this to be irrelevant within the μSR time window, but it plays a role for the relaxation behavior of the remanent magnetization (see Ref. 49).
[53]F. Schwarzl and A. J. Staverman, Physica **18**, 791 (1952); Appl. Sci. Res. A **4**, 127 (1953).
[54]A. P. Murani, F. Mezei, and J. L. Tholence, Physica B+C **108B**, 1283 (1981).
[55]Dynamic mean-field theory predicts a spin-autocorrelation function similar to Eq. (7) with $S_d(t) \propto t^{-\gamma}$, where $\gamma = \beta/(\nu z)$ is the equivalent exponent to $1/(\delta x)$ in the fractal cluster model (see Refs. 35 and 36).
[56]J. H. Brewer and K. M. Crowe, Ann. Rev. Nucl. Part. Sci. **28**, 239 (1978).
[57]A. Seeger, in *Topics in Applied Physics* (Springer, Heidelberg, 1978), Vol. 28, p. 349.
[58]A. B. Denison, H. Graf, W. Kündig, and P. F. Meier, Helv. Phys. Acta **52**, 460 (1979).
[59]P. F. Meier, in *Exotic Atoms '79,* edited by K. M. Crowe, J. Duclos, G. Fiorentini, and G. Torrelli (Plenum, New York, 1979), p. 355.
[60]Y. M. Belusov, V. N. Gorelkin, A. N. Mikaelyan, V. Y. Miloserdin, and V. P. Smilga, Usp. Fiz. Nauk **129**, 3 (1979) [Sov.—Phys. Usp. **22**, 679 (1979)].
[61]S. F. J. Cox, J. Phys. C **20**, 3187 (1987).
[62]A. Schenck, *Muon Spin Rotation Spectroscopy* (A. Hilger, Bristol, 1985).
[63]See, e.g., J. Chappert, A. Yaouanc, O. Hartmann, E. Karlsson, L. O. Norlin, and T. O. Niinikoski, Solid State Commun. **44**, 13 (1982); R. Kadono, T. Matsuzaki, K. Nagamine, T. Yamazaki, D. Richter, and J. M. Welter, Hyperfine Interact. **31**, 205 (1986).
[64]R. H. Heffner, Hyperfine Interact. **8**, 655 (1981).
[65]M. R. McHenry, B. G. Silbernagel, and J. H. Wernick, Phys. Rev. B **5**, 2958 (1972).
[66]R. E. Walstedt and L. R. Walker, Phys. Rev. B **9**, 4857 (1974).
[67]A. L. Mikaelyan and V. P. Smilga, Zh. Eksp. Teor. Fiz. **81**, 2324 (1981) [Sov. Phys.—JETP **53**, 1216 (1981)].
[68]Y. J. Uemura, Ph. D. thesis, University of Tokyo (1982).
[69]T. Yamazaki, Hyperfine Interact. **6**, 115 (1979).
[70]R. Kubo, Hyperfine Interact. **8**, 731 (1981).
[71]Y. J. Uemura and T. Yamazaki, J. Magn. Magn. Mater. **31–34**, 1359 (1983).
[72]R. H. Heffner, M. Leon, M. E. Schillaci, D. E. MacLaughlin, and S. A. Dodds, J. Magn. Magn. Mater. **31–34**, 1363 (1983).
[73]A. Abragam, *The Principles of Nuclear Magnetism,* 6th ed. (Oxford University Press, Oxford, 1961).
[74]R. Kubo and T. Toyabe, in *Magnetic Resonance and Relaxation,* edited by R. Blinc (North-Holland, Amsterdam, 1967), p. 810.
[75]See, e.g., C. W. Clawson, K. M. Crowe, S. E. Kohn, S. S. Rosenblum, C. Y. Huang, J. L. Smith, and J. H. Brewer, Physica B+C **109+110B**, 2164 (1982); R. Kadono, J. Imazato, K. Nishiyama, K. Nagamine, and T. Yamazaki, Hyperfine Interact. **17–19**, 109 (1984).
[76]R. Kubo, J. Phys. Soc. Jpn. **9**, 935 (1957).
[77]R. S. Hayano, Y. J. Uemura, J. Imazato, N. Nishida, T. Yamazaki, and R. Kubo, Phys. Rev. B **20**, 850 (1979).
[78]D. E. Murnick, A. T. Fiory, and W. J. Kossler, Phys. Rev. Lett. **36**, 100 (1976).
[79]R. H. Heffner, D. W. Cooke, R. L. Hutson, M. E. Schillaci, S. A. Dodds, G. A. Gist, and D. E. MacLaughlin, J. Magn. Magn. Mater. **54–57**, 1103 (1986).
[80]Y. J. Uemura, T. Yamazaki, D. R. Harshman, M. Senba, and E. J. Ansaldo, Phys. Rev. B **31**, 546 (1985).
[81]The form of Eq. (16) deviates from the usual "decay of the $\frac{1}{3}$ tail" (e.g., Refs. 7 and 77), but yields better agreement to the "Lorentzian strong collision model" (Ref. 6).
[82]H. Pinkvos, Ph.D. thesis, Technical University of Braunschweig (1988).
[83]Another (spatial) distribution of correlation times was found to be unsuitable for the interpretation of longitudinal field μSR measurements below T_f by Y. J. Uemura and T. Yamazaki, Physica B+C **109+110B**, 1915 (1982). The distribution used in that work corresponds to a Gaussian curve in Fig. 1 and was not inferred from a particular spin-glass theory.
[84]K. Emmerich, E. Lippelt, R. Neuhaus, H. Pinkvos, Ch. Schwink, F. N. Gygax, A. Hintermann, A. Schenck, W. Studer, and A. J. van der Wal, Phys. Rev. B **31**, 7226 (1985).
[85]H. Pinkvos, F. N. Gygax, E. Lippelt, R. Neuhaus, A. Schenck, Ch. Schwink, and A. J. van der Wal, Hyperfine Interact. **31**, 363 (1986).
[86]D. E. MacLaughlin, L. C. Gupta, D. W. Cooke, R. H. Heffner, M. Leon, and M. E. Schillaci, Phys. Rev. Lett. **51**, 927 (1983).
[87]Y. J. Uemura, K. Nishiyama, T. Yamazaki, and R. Nakai, Solid State Commun. **39**, 461 (1981).
[88]G. A. Gist and S. A. Dodds, Phys. Rev. B **30**, 2340 (1984).
[89]We have used the values $S = \frac{5}{2}$ and $g_{\text{eff}} = 1.72$ for *Cu*Mn and $g_{\text{eff}} = 1.85$ for *Au*Mn, which may be obtained from Ref. 10 and from A. F. J. Morgownik, J. A. Mydosh, and C. van Dijk, J. Magn. Magn. Mater. **31-34**, 1334 (1983).
[90]To account for the different absolute field amplitudes, we have scaled the λ_d values for the *Au*Mn samples by $K^2(CuMn)/K^2(AuMn)$ from Eq. (29).
[91]Calculating the values of τ_{eff} directly from Eq. (30) increases the error bars considerably because of the large uncertainty associated with q_H (see Fig. 13), thus making the comparison somewhat less convincing than the procedure applied in Fig. 10.

[92]J. Souletie and R. Tournier, J. Low Temp. Phys. **1**, 95 (1969).

[93]From the relation $\delta x = \nu z/\beta$ (Ref. 47), we have also $w = \nu z - \beta$, which is far more general than our derivation from the fractal cluster mode might suggest, see Ref. 36.

[94]See, e.g., M. Fähnle, W.-U. Kellner, and H. Kronmüller, Phys. Rev. B **35**, 3640 (1987).

[95]The decrease of τ_{eff} below T_f was also qualitatively mentioned in Ref. 80, but no further attempts were made to interpret this effect.

[96]A. Mukhopadhyay and P. A. Beck, Solid State Commun. **16**, 1067 (1975).

[97]S. Crane and H. Claus, Solid State Commun. **35**, 461 (1980).

[98]T. J. Aton, T. S. Stakelon, and C. P. Slichter, Phys. Rev. B **18**, 3337 (1978).

[99]In this context the quenching procedure was overemphasized by Y. J. Uemura, Hyperfine Interact. **8**, 739 (1981).